



Study on the deformation and fracture of epoxy monoliths through mechanical tensile and compressive tests and X-ray CT imaging

Kazuma Aragishi¹ · Yoshihiro Takeda² · Yasuhito Suzuki¹ · Akikazu Matsumoto¹

Received: 11 October 2023 / Revised: 1 December 2023 / Accepted: 3 December 2023 / Published online: 11 January 2024
© The Society of Polymer Science, Japan 2024

Abstract

As porous polymer materials with continuous epoxy skeletons and pores, epoxy monoliths are used as column fillers in HPLC, separators in lithium-ion batteries, and precursor polymers for monolith adhesion and co-continuous network polymer fabrication. Due to their unique mechanical properties and fracture behavior, epoxy monoliths can incur large deformation and are different from the bulk thermoset of epoxy resins that exhibit hard and brittle features. In this study, we prepared an epoxy monolith using 2,2'-bis(4'-glycidylphenoxy)propane (BADGE) and tripropylene glycol diglycidyl ether (TPGD) as epoxy resins, 4,4'-methylenebis(cyclohexylamine) (BACM) as a crosslinker, and poly(ethylene glycol) (PEG) as a porogen, and TPGD-induced effects on the pore structure and properties of the obtained monoliths were investigated. To clarify the relationship between the pore structure and the mechanical properties of the monolith, scanning electron microscopy (SEM) observations and tensile and compression tests were performed. In addition, X-ray CT imaging nondestructively revealed a change in the inner porous structure of the monolith after a large deformation occurred under various compression conditions. We clarified the effects of the TPGD addition on the monolith structure and the mechanical properties with tensile and compressive deformation.

Introduction

Epoxy resins are among the most widely used thermosetting resins in various applications, such as adhesives, coatings, and fiber-reinforced composites, in electronics, automotives, and aerospace fields, as the resins exhibit excellent mechanical and thermal properties, chemical resistance, corrosion resistance, electric insulation, low dielectric constants, and low shrinkage

[1–8]. Glassy and highly crosslinked polymer materials, such as epoxy resins, exhibit no creep; however, these materials involve a brittle fracture problem due to a lack of polymer chain slippage. It was reported that adding elastomers as energy absorbers effectively toughens hard epoxy resins by suppressing crack propagation at a crack tip [9–11]. As previously clarified, epoxy resins can be toughened by cavitating an elastomer phase and subsequently deforming the plastic of the epoxy matrix [11].

Epoxy monoliths are porous polymer materials with continuous epoxy skeletons and pores [12, 13], which are used as column fillers in high-performance liquid chromatography (HPLC) [14, 15] and as separators in lithium-ion batteries [16]. Recently, we developed a monolith bonding system that is effective for dissimilar material bonding, such as metal–polymer bonding [17–19]. Using this method, the bonding strength increases due to an anchoring effect, which resulted from the penetration of the polymer into pores of the epoxy monolith as an adhesion layer applied to the metal surfaces. Furthermore, new types of polymer composites, i.e., co-continuous network polymers (CNPs), were fabricated by filling the continuous pores of epoxy monoliths with any other epoxy resin, thiol–ene thermosetting resin, or polyacrylate as second polymer components

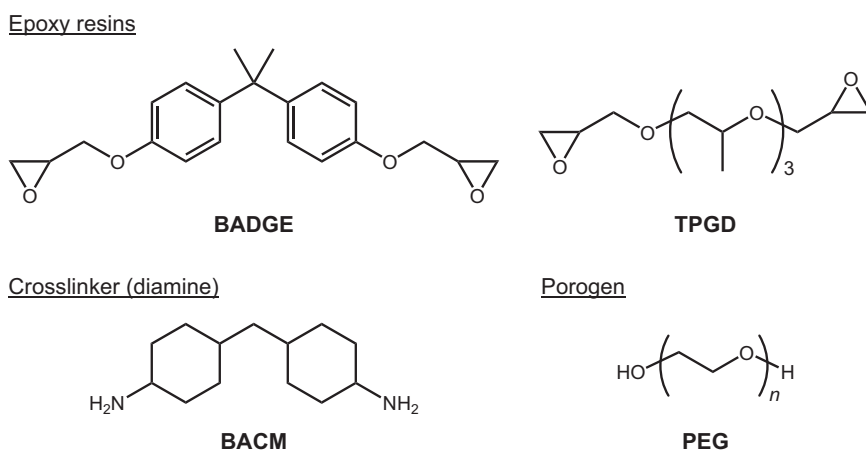
Supplementary information The online version contains supplementary material available at <https://doi.org/10.1038/s41428-023-00872-8>.

- ✉ Yasuhito Suzuki
suzuki_y@omu.ac.jp
- ✉ Akikazu Matsumoto
akimatsumoto@omu.ac.jp

¹ Department of Applied Chemistry, Graduate School of Engineering, Osaka Metropolitan University, 1-1, Gakuen-cho, Naka-ku, Sakai, Osaka 599-8531, Japan

² Advanced Analysis Research Department, X-Ray Research Laboratory, Rigaku Corporation, 3-9-12, Matsubara-cho, Akishima, Tokyo 196-8666, Japan

Fig. 1 Chemical structure of the materials used in this study



with a crosslinked structure [20, 21]. The CNPs are very strong due to the combination of epoxy monoliths with a high glass transition temperature (T_g) and second network polymers with a low T_g . Effective energy dissipation occurs according to a fracture mechanism based on sacrificial bonds. The epoxy monolith exhibited an elastic property in a small deformation range during a tensile test, followed by plastic deformation and the partial fracture of the epoxy monolith backbone in a larger deformation range. The tensile deformation finally reached the macroscopic destruction of the entire samples. In our previous studies on the fracture mechanism of epoxy monoliths and CNPs [21], the fracture position could not be controlled at the final stage of each tensile test because the stress was concentrated at several specific positions and macroscopic cracks advanced suddenly at an unexpected position. Therefore, it is difficult to consistently track deformation and fracture phenomena from the microscopic deformation of the monolith skeleton to macroscopic fracture of the entire sample under tensile stress conditions.

In this study, we first prepared sheet- and cylinder-type epoxy monoliths, which were available for mechanical tensile and compression tests, respectively, using 2,2'-bis(4'-glycidyloxyphenyl)propane (BADGE) and tripropylene glycol diglycidyl ether (TPGD) as the epoxy resins, 4,4'-methylenebis(cyclohexylamine) (BACM) as the crosslinker, and poly(ethylene glycol) (PEG) as the porogen (Fig. 1), according to a fabrication process described in a previous report [21]. Epoxy bulk thermosets without a porous structure were also prepared as reference materials. Then, their thermal properties were investigated by differential scanning calorimetry (DSC) and dynamic mechanical analysis (DMA), and the porous structure of the epoxy monolith fabricated under various conditions was observed by scanning electron microscopy (SEM). The X-ray CT imaging method [19–23] was also used to nondestructively observe a change in the inner porous structure with a large deformation under applied compressive force conditions.

Here, we clarify the effects adding TPGD on the monolith structure and mechanical properties with tensile and compressive deformation.

Experimental methods

Materials

BADGE (>85%), BACM (>97%), and PEG (number-average molecular weight 200) were purchased from Tokyo Chemical Industry Corporation, Ltd., Tokyo, Japan, and used as received. Poly(vinyl alcohol) (PVA, the degree of polymerization 500) was purchased from Nacalai Tesque, Inc., Kyoto, Japan, and used as received. TPGD was commercially available as SR-TPG by Sakamoto Yakuhin Kogyo Corporation Ltd., Osaka, Japan, and used without further purification.

Preparation of epoxy monolith sheets

The epoxy monolith sheets were fabricated as follows. BADGE, TPGD, BACM, and PEG were mixed for 15 min using a planetary centrifugal mixer (AR-100, Thinky Corporation, Tokyo, Japan) at ratios of $2[\text{NH}_2]/[\text{epoxy}]$ (i.e., γ value) = 1.4 and 70 wt% PEG. The mixed paste of the reactants was spread on a PVA-coated glass plate and provided for thermal curing in an oven at 120 °C for 1.5 h (VOC-210SD, Tokyo Rikakikai (EYELA) Corporation, Ltd., Tokyo, Japan). After curing, the samples were washed with ion-exchanged water by ultrasonication for 5 min to remove the PEG, stored in ion-exchanged water overnight, and then dried in vacuo at room temperature.

Preparation of epoxy monolith cylinders

The cylindrical epoxy monoliths were typically fabricated as follows. BADGE, TPGD, BACM, and PEG were mixed for

15 min using a planetary centrifugal mixer at $\gamma = 1.4$ and 70 wt% PEG. The mixed paste was placed in a 4.1 mm-diameter glass vial and heated in an oil bath at 100–140 °C for 1.5 h. After curing, the samples were isolated from the glass-ware, washed with ion-exchanged water by ultrasonication to remove the PEG, stored in ion-exchanged water overnight, and then dried in vacuo at room temperature. The isolated rod-shaped samples were cut to an appropriate length.

Preparation of bulk epoxy thermosets

The bulk epoxy thermosets were fabricated in the absence of porogen in a 120 °C oven for 1.5 h, according to procedures similar to those used to prepare epoxy monoliths. The γ value was 1.4 or 1.0. The bulk epoxy thermosets were produced as sheet and cylindrical test pieces.

General procedures

SEM observation was performed using a VE-9800 (Keyence Corporation, Ltd., Osaka, Japan) with an acceleration voltage of 1.0–20 kV with or without Au vapor deposition using an MPS-1S magnetron sputtering chamber (Vacuum Device Corporation, Mito, Ibaraki, Japan). DMA was carried out using a DMS 6100 (SII Nanotechnology, Tokyo, Japan). The size of the test pieces was 10 mm \times 40 mm \times ca. 0.3 mm. The precise thickness was determined using a Peacock dial thickness gauge (Ozaki Mfg. Corporation, Ltd., Osaka, Japan). The measurement conditions were a dual cantilever mode at a heating rate of 2 °C/min. Sinusoidal strains with an amplitude of 10 μ m at 1 Hz were applied. The T_g was determined as the peak temperature of the $\tan\delta$ curves. DSC measurements were carried out to determine the T_g using a Discovery DSC250 (TA Instruments-Waters, USA) at a heating rate of 10 °C/min in a nitrogen stream.

X-ray CT imaging

X-ray CT imaging was carried out using a CTnano3DX X-ray microscope (Rigaku Corporation, Tokyo, Japan) equipped with a Cu target (K_α , $\lambda = 0.15418$ nm, 8.048 keV, tube voltage 40 kV, tube current 30 mA). The sample was placed on a 2-axis goniometer stage. The field of view (FOV) for the camera was 0.66 mm \times 0.66 mm, and the effective pixel was 0.62 μ m. The goniometer stage was rotated 180 degrees, and 600 projection images were taken. The scan time was 15–60 min. The Feldkamp–Davis–Kress (FDK) algorithm was then used to reconstruct the tomograms [21].

Tensile and compression tests

The tensile and compression tests were carried out using an Autograph AGS-X 1 kN (Shimadzu Corporation, Ltd., Kyoto,

Japan) at room temperature and a tensile or compression rate of 1.0 mm/min. The size of the sheet-type test pieces used for the tensile test was 10 mm \times 40 mm. The thickness of the test pieces was ca. 300 μ m. The precise thickness was determined using a Peacock dial thickness gauge. Cylindrical test pieces with 3.3–3.8 mm ϕ \times 5.5–6.5 mm height and 4.0–4.1 mm ϕ \times 5.1–6.5 mm height for the monoliths and the bulk thermosets, respectively, were used for the compression test. The Young's modulus was determined from the initial slope of the stress–strain curves (1–2% in elongation). An apparent cross-sectional area of the samples at an initial stage was used to calculate the modulus because the Poisson's ratio was unavailable for the monoliths. The strength and modulus values of the epoxy monoliths were calculated without correcting the cross-sectional area due to the included pores. The cycle number was 10 for the cyclic compression test.

Results and discussion

Pore structure and tensile property of monolith sheets

We prepared epoxy monolith sheets using BADGE and TPGD as epoxy resins in combination with BACM and PEG under curing conditions of γ (a ratio of the number of amino hydrogens to an epoxy group) = 1.4 at 120 °C for 1.5 h. The effects of adding TPGD on the porous structure and the mechanical properties of the obtained monolith sheets were investigated. In our previous study [21], it was revealed that the average pore size and the diameter of the epoxy monolith skeleton increased with an increase in the γ values and a decrease in the curing temperature. Furthermore, the added TPGD tended to decrease the pore size, but the detailed effect was not clear. In this study, the γ value for monolith fabrication was fixed at 1.4. The common manufacturing process for epoxy thermosets requires a stoichiometric ratio of epoxy and amine (i.e., $\gamma = 1.0$) for the formation of a well-developed network structure, leading to the appearance of high strength and toughness of the thermosets. To evaluate the effect of TPGD addition on the pore sizes, an epoxy monolith with a coarse framework is needed. The coarse monolithic framework is also advantageous for X-ray CT analysis. By monitoring the unreacted epoxy groups at 916 cm^{-1} in the IR spectrum, we confirmed that the fast ring-opening reaction of epoxy groups occurred during the preparation of epoxy monoliths with $\gamma = 1.0$ and 1.4 in the absence and presence of TPGD at 120 °C, as shown in Fig. 2a. The epoxy groups were mostly consumed within 20 min, and the reaction achieved a constant value of ~90% conversion (Fig. 2b). The consumption rate of the epoxy moiety was independent of the TPGD content. The initial consumption rate of the epoxy group was slightly

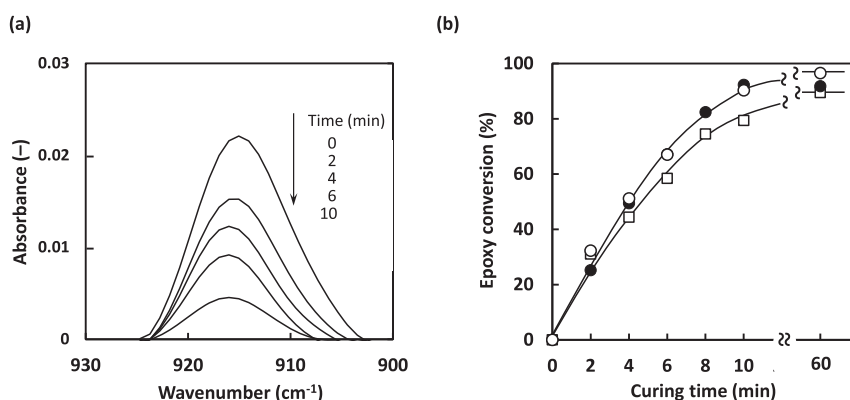
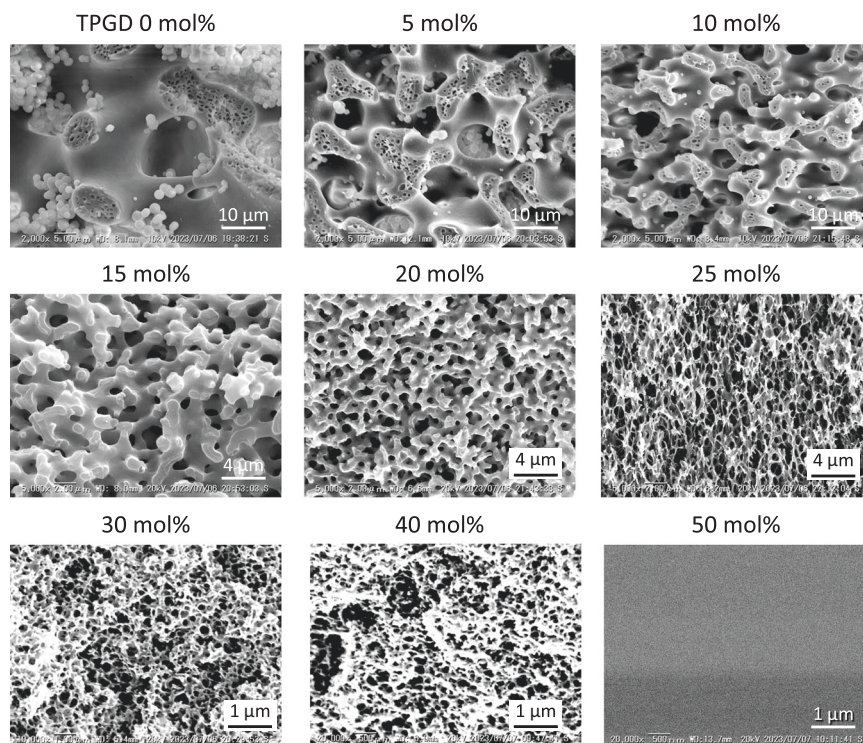


Fig. 2 **a** Change in the characteristic peak observed at 916 cm^{-1} due to an epoxy group in the IR spectrum of the BADGE/BACM/PEG curing system at $120\text{ }^{\circ}\text{C}$ (TPGD $0\text{ mol}\%$, $\gamma = 1.0$). **b** Time-conversion relationship for the reaction for the BADGE/BACM/PEG curing systems

in the absence and presence of TPGD at $120\text{ }^{\circ}\text{C}$. (○) TPGD $0\text{ mol}\%$, $\gamma = 1.4$, (●) TPGD $40\text{ mol}\%$, $\gamma = 1.4$, and (□) TPGD $0\text{ mol}\%$, $\gamma = 1.0$. Solid curves are guides to the eye

Fig. 3 Cross-sectional SEM images of the inner structure of the epoxy monolith sheets prepared at $120\text{ }^{\circ}\text{C}$ for 1.5 h in the presence of different amounts of TPGD ($0\text{--}50\text{ mol}\%$). The γ value was 1.4



higher in the presence of an excess amount of amine at $\gamma = 1.4$ than that observed under stoichiometric conditions. These results support that the curing reactions of all epoxy monoliths fabricated in this study were complete under heating conditions at $120\text{ }^{\circ}\text{C}$ for 1.5 h , independent of the γ values.

Figure 3 shows cross-sectional SEM images of the inner structure of the epoxy monoliths prepared at different TPGD contents. Both sizes of the pores and the monolith skeleton thickness drastically decreased after TPGD was added because hydrophilic TPGD suppressed phase

separation and retarded the subsequent Ostwald ripening, resulting in the formation of epoxy monoliths with a fine pore structure. The pore and epoxy skeleton sizes were several tens of μm in the absence of TPGD, while they became submicron order when over $20\text{ mol}\%$ TPGD was added. Adding $50\text{ mol}\%$ TPGD resulted in a nonporous structure, as shown in the SEM image. The transparency of the produced epoxy sheet increased based on visual observations. These results suggest that a nonporous structure was formed because phase separation did not occur during the epoxy curing process. Otherwhile,

nanopores were produced, which may be difficult to detect by SEM observation or by the scattering of visible light with the naked eye.

In this study, we further confirmed that a large number of globules with a few μm diameter as curing products were formed in the porous area of the epoxy monoliths when the monoliths were fabricated without TPGD (Fig. 3). The formation of globules may result from secondary phase separation, which occurred in a porogen-rich phase produced after spinodal decomposition, generating the main monolith structure [15, 24]. At the same time, another spherical pore structure was observed in the epoxy monolith skeletons, which was also created by secondary phase separation consisting of a porogen-rich component. It has been reported that similar hierarchical macro- and mesoporous structures occur for silica monoliths, and they are useful as ultrahigh-performance column fillers for GC and HPLC [25, 26]. These small pores of the monoliths play an important role for chromatographic separation. The secondary epoxy globules were only formed when the TPGD content was less than 20 mol%, while adding a larger amount of TPGD suppressed the formation of small globules and pores.

The addition of TPGD influenced not only the pore structure but also the mechanical properties of the monoliths. The results for the mechanical tensile test of monolith sheets prepared by the fabrication conditions at various TPGD contents are summarized in Table 1. In our previous reports [20, 21], it was confirmed that an increase in the

amount of BACM, i.e., an increase in the γ value, led to the predominant propagation of the linear polymer chain rather than branch formation and crosslinking. This resulted in the formation of a loose network structure of the epoxy resins, which exhibited greater stretchable properties. In the present study, we successfully demonstrated that the TPGD content changed the mechanical properties of the monolith sheets. Typical stress–strain curves for the epoxy monolith sheets with various TPGD contents are shown in Fig. 4. In each stress–strain curve, an inflection point (like a yielding point) was observed at the initial strain region, although the epoxy monolith skeletons consist of crosslinked network polymers with less molecular slipping. The strength and strain values at an inflection point are summarized in Table 1. This inflection point was not observed for the corresponding epoxy bulk thermosets because they were not stretchable and were fractured at less than several percent strain [20, 21].

Changes in the maximum strength and strain at breakage as well as the Young's modulus as a function of the TPGD content are depicted in Fig. 5. When a small amount of TPGD was added, the maximum strength slightly increased from 9.1 ± 1.1 MPa to 10.3 ± 1.7 MPa along with the addition of 10 mol% TPGD. Then, the strength gently decreased to 8.8 ± 0.7 MPa at 20 mol% TPGD addition. The addition of more than 20 mol% TPGD discontinuously decreased the maximum strength in the range of 4.0–4.7 MPa. The strengths were approximately half the strength attained for the monoliths without TPGD or with less than 20 mol% TPGD. The Young's modulus also discontinuously decreased. The values in a range less than 20 mol% of TPGD (434–544 MPa) were binarized as 198–271 MPa in a range more than 20 mol%. The strength and modulus values

Table 1 Tensile mechanical properties of monolith sheets including various amounts of TPGD^a

TPGD content (mol%)	Young's modulus (MPa)	Maximum strength (MPa)	Strain at break (%)	At the inflection point	
				Strength (MPa)	Strain (%)
0	434 ± 61	9.1 ± 1.1	23.6 ± 4.2	7.2 ± 1.0	1.5 ± 0.2
5	514 ± 28	9.6 ± 0.4	29.3 ± 4.5	7.3 ± 0.7	1.4 ± 0.1
10	513 ± 61	10.3 ± 1.7	30.3 ± 7.5	9.5 ± 1.6	1.8 ± 0.3
15	544 ± 51	9.8 ± 1.4	19.3 ± 3.4	8.8 ± 1.3	1.6 ± 0.3
20A ^b	452 ± 22	8.8 ± 0.7	14.9 ± 4.0	8.4 ± 0.6	1.9 ± 0.2
20B ^b	241 ± 21	4.7 ± 0.4	16.1 ± 3.3	4.6 ± 0.4	1.5 ± 0.2
25	243 ± 30	4.2 ± 0.5	6.4 ± 1.4	^c	^c
30	198 ± 24	4.0 ± 0.7	5.4 ± 1.1	^c	^c
40	271 ± 28	4.5 ± 0.5	3.9 ± 0.6	^c	^c
50	92 ± 14	3.6 ± 0.3	119 ± 17	2.3 ± 0.2	1.2 ± 0.0

^aEpoxy monolith sheets were prepared using BADGE and TPGD as epoxy resins and BACM as a cross-linker in the presence of PEG as a porogen under the conditions of $\gamma = 1.4$ at 120 °C for 1.5 h

^bEpoxy monoliths produced at 20 mol% TPGD were divided into two groups with or without the formation of secondary epoxy particles. The mechanical properties were evaluated for each group

^cNot determined

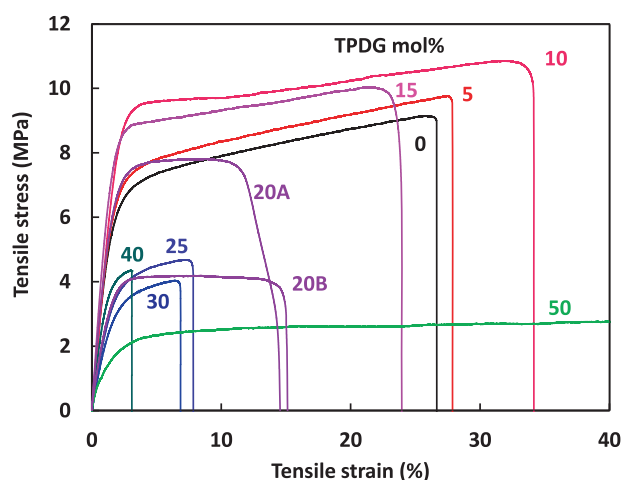


Fig. 4 Typical stress–strain curves for the tensile test of monolith sheets (TPGD content 0–50 mol%) at room temperature and a tensile rate of 1.0 mm/min. See the footnote in Table 1 for the samples of 20A and 20B

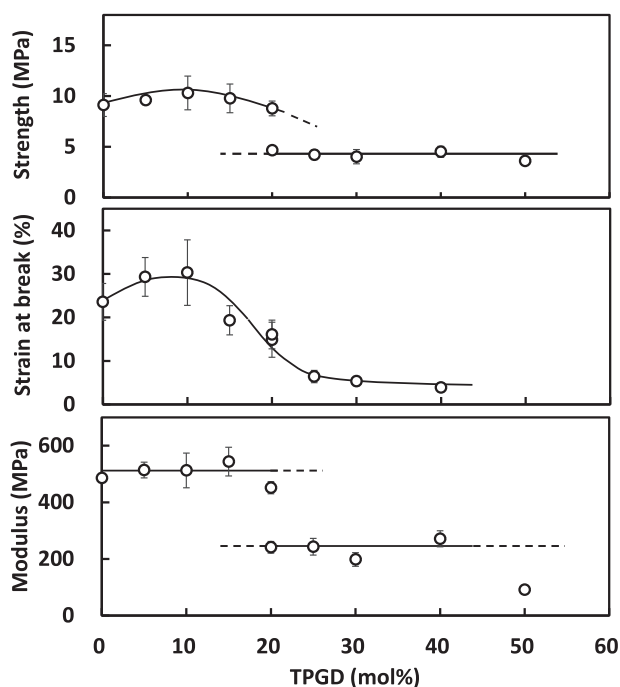


Fig. 5 Effects of the TPGD content on maximum strength, strain at break, and Young's modulus for the tensile test of the monolith sheets prepared using BADGE and TPGD as the epoxy resins and BACM as the crosslinker in the presence of PEG as the porogen. Solid curves are guides to the eye

of the epoxy monoliths were determined without correction of the cross-sectional area, although the monoliths contained a considerable volume of pores. The volume porosity was estimated to be 43–49% in our previous study [21]. The estimated elastic moduli of the monolith (0.2–0.5 MPa) were much lower than those of the bulk thermosets (1.1–2.4 GPa) reported in this and previous studies. The modulus values of the epoxy monolith were lower than those expected from bulk thermosets, even if the cross-sectional area was corrected. This is because the deformation of the epoxy monoliths mainly occurs by the bending and twisting of the monolith frameworks rather than the stretching of epoxy materials at the initial stage of deformation.

In this study, it was found that the epoxy monoliths produced at a TPGD content of 20 mol% were clearly divided into two classes of materials; one class included the formation of spherical particles with a few μm diameter and the other contained no spherical particles, as shown in the SEM images in Fig. 3. As a result, the mechanical properties of the monolith sheet samples prepared at 20 mol% TPGD content can be separated into two groups, as shown in the stress–strain curves in Fig. S1 in the Supplementary Materials. This explains the discontinuous relationships in the TPGD content and the maximum strength or the Young's modulus in Fig. 5.

Notably, adding a large excess amount of TPGD, such as 50 mol%, resulted in a drastic decrease in the T_g of the produced monolith, which was in the rubbery state at room temperature. This resulted in an extreme decrease in the Young's modulus to less than 100 MPa as well as a remarkably large elongation over 100%.

The change in the mechanical properties of the monolith with the addition of TPGD was interpreted based on several factors. The most important factor is the plasticizing effect due to flexible TPGD segments that were incorporated into the polymer backbone. The second factor is a change in the molecular network structures of crosslinked epoxy polymers. The third is a change in the macroscopic sizes of the monolith skeletons in the micrometer order, which resulted from suppressed phase separation in the presence of TPGD. The effect of the secondary small epoxy particles on the mechanical properties is not negligible. In this study, the sizes of epoxy monoliths and pores were not precisely evaluated due to the two-step phase separation and the complicated monolith structures, as shown in Fig. 3. The sizes of the monolith skeletons and the pore may show a discontinuous change at the boundary of 20 mol% TPGD content, which can sensitively switch the phase separation behavior during the epoxy curing process. We are continuing to suppress the formation of globular aggregates during the fabrication of epoxy monoliths.

To investigate a plasticizing effect and changes in the molecular network structure by the addition of TPGD, the thermal and mechanical properties of the corresponding bulk thermosets (including TPGD), which were prepared in the absence of the porogen under similar curing conditions, were evaluated by DMA measurements. Typical DMA curves for the bulk thermosets prepared in the presence and absence of TPGD are shown in Fig. 6. The effects of adding TPGD on the DMA parameters are summarized in Table 2. The T_g value, which was estimated based on the peak temperature of the $\tan\delta$ values in the DMA curves, decreased from 123 °C to 68 °C. In addition, along the TPGD content increased from 0 to 25 mol% due to the flexibility of the TPGD segment that contained a tripropylene glycol structure. In contrast, the E' value in the glassy state under T_g of the epoxy thermosets was constant at 1.08–1.49 GPa independent of the TPGD content. The flexibility of the TPGD segment had a negligible effect on the elastic property of the epoxy thermosets in the glassy state at room temperature, which is much lower than T_g .

On the other hand, the E' value in the rubbery state over T_g decreased from 17.7 MPa to 4.87 MPa as the TPGD content increased from 0 to 25 mol%. The change in E' values in the rubbery state indicates that the crosslinking density decreases and the average molecular weight between the crosslinking points increases when TPGD is

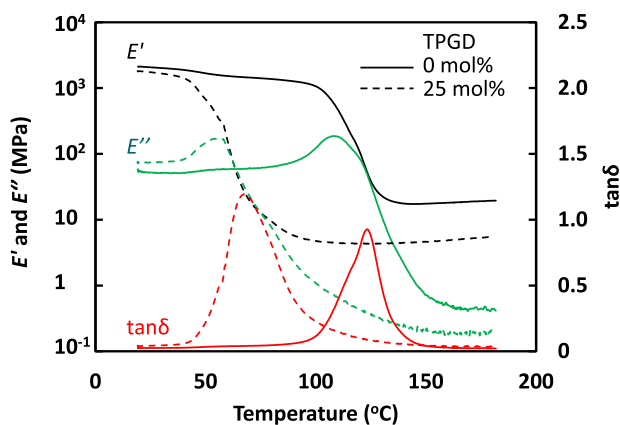


Fig. 6 DMA curves for epoxy bulk thermosets prepared using BADGE and BACM in the absence and presence of TPGD

added. BADGE and TPGD contain the same glycidyl group as the functional group at both ends of the molecule, but the mobility of the glycidyl groups of TPGD is much higher than that of BADGE with a rigid molecular structure during the curing reaction. The reaction kinetics of amino and hydroxy groups formed in the polymer chains by the ring-opening reaction may depend on the length and flexibility of the space between the functional groups in the polymer networks. However, the consumption rate of the epoxy moiety was constant and not dependent on the absence or presence of TPGD, as shown in Fig. 2. Based on the DMA results, it can be concluded that adding TPGD resulted in the formation of epoxy thermosets with a looser network structure according to the TPGD content. Therefore, the chain extension may be preferred by the reaction between the primary amine on the polymer chain ends and the epoxy moiety rather than the branching and crosslinking reactions by the secondary amine on the polymer main chain. It was difficult to separately evaluate these reactions by the primary and secondary amines using the kinetic data shown in Fig. 2.

When the T_g values of the epoxy monoliths and the bulk thermosets were evaluated by DSC, several significant results were revealed. As shown in Fig. 7, the T_g values for the epoxy monoliths and the bulk thermosets decreased according to the increase in the TPGD content, as expected. The T_g values of the monoliths and the bulk thermosets were consistent with each other for the samples that contained over 20 mol% TPGD. In contrast, the T_g values of the monolith were clearly lower than those of the bulk thermosets in regions containing less than 20 mol% TPGD. This indicates that PEG used as a porogen exhibits a plasticizing effect. A considerable amount of PEG remained in the epoxy skeletons after the procedure for removal was performed as the epoxy monoliths were fabricated. This plasticizing effect was solely observed for the monoliths prepared under fabrication conditions with less

Table 2 DMA data for epoxy bulk thermosets prepared using BADGE and TPGD as the epoxy resins and BACM as the crosslinker without porogen

TPGD content (mol%)	$T_g^{a,b}$ [DSC] (°C)	T_g^c [DMA] (°C)	E' in the glassy state ^d (GPa)	E' in the rubbery state ^e (MPa)	$M_c^f \times 10^{-3}$ (g/mol)
0	112 (71)	123	1.22	17.7	0.66
5	100 (59)	109	1.11	8.58	1.3
10	72 (55)	100	1.08	9.30	1.2
15	62 (61)	91	1.32	9.41	1.2
20	67 (40)	77	1.13	5.21	2.0
25	45 (53)	68	1.49	4.87	2.1

^aDetermined by DSC

^bValues in parentheses indicate T_g for epoxy monoliths, determined by DSC

^cDetermined as a peak temperature of $\tan \delta$

^dDetermined at a temperature of $T_g - 30$ °C

^eDetermined at a temperature of $T_g + 30$ °C

^fAverage molecular weight between cross-linking points, calculated with an assumption that the density is 1.1 g/ml

than 20 mol% TPGD content, in which secondary phase separation occurred.

As shown in Figs. 4 and 5, the strain values at break slightly increase in the range with a smaller amount of TPGD and exhibit a maximum at 10 mol%, then the strain continuously and rapidly decreased with an increase in the TPGD content. This process differs from the changes observed in the strength and the Young's modulus (see Fig. 5). For the fracture of the monolith sheets, the microscopic damage at the local positions of the epoxy monolith accumulates, and the macroscopic breakdown at a certain location, in which stress is concentrated. For general materials with a simple and homogeneous component, a decrease in the T_g values due to the soft segments introduced leads to a decrease in the Young's modulus and an increase in the strain value at break. However, it was clarified that the deformation behavior of the monoliths as porous materials was complicated during the tensile test. In this study, therefore, a compression test was carried out to continuously track the deformation behavior from an initial structural change in the monolith skeletons to a final fracture of the materials under high compressive pressure conditions.

Compressive response of epoxy monolithic cylinders

When we first tried to manufacture a cylindrical sample of the epoxy monoliths using test tubes with a diameter of 8 or 12 mm, the isolated compounds obtained after curing contained a heterogeneous and complicated inner structure. For these samples, a porous monolith structure was confirmed at

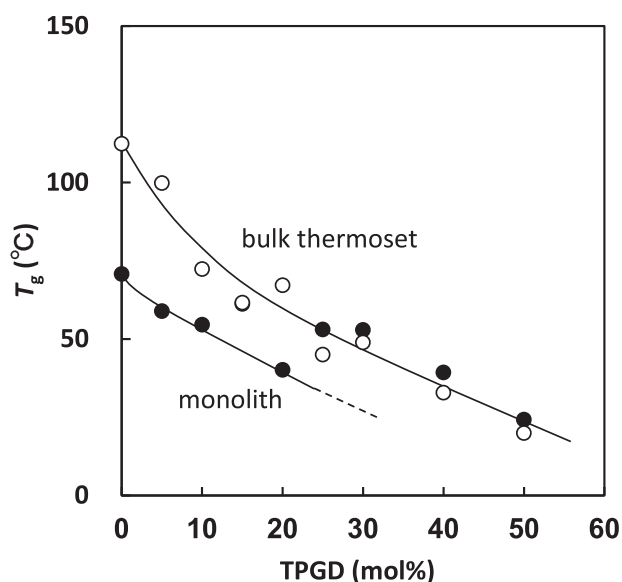


Fig. 7 Changes in the T_g values for (●) epoxy monoliths and (○) bulk thermosets as a function of the TPGD content. The T_g was determined by DSC at a heating rate of 10 °C/min in a nitrogen stream. Solid curves are guides to the eye

several positions of the products, but marble-like or winding stratum-like structures were simultaneously observed, as shown in Figs. S3 and S4 in the Supplementary Materials. This unexpected and artistic structure was probably produced by heterogeneous temperature distribution, i.e., a localized rise in the temperature during the exothermic curing reactions of epoxy resins due to a low heat conductivity. The rapid increase in temperature led to the acceleration of heterogeneous phase separation and liquid convection to produce marble or stratum-like structures. Interestingly, this heterogeneous structure was not observed in the epoxy monolith sheets that were fabricated in a temperature-controlled oven because the generated heat could easily diffuse from the surfaces of sheets with an ~0.3 mm thickness. The heat accumulation at a local position induces a subsequent acceleration in the reactions and phase separation, which is disadvantageous for the preparation of cylindrical epoxy monolith samples with a large size. Eventually, we successfully fabricated epoxy monoliths with a uniform porous structure as cylindrical samples with a 4-mm diameter by heating using an oil bath, but not an oven.

In this study, the mechanical compression test was carried out using cylindrical samples of epoxy monoliths and thermosets with a size of 3.3–3.8 mm ϕ \times 5.5–6.5 mm height. The stress–strain curves for each sample containing different TPGD contents are shown in Fig. 8. The characteristic parameters determined from the stress–strain curves are summarized in Table 3. The compressive deformation profiles showed several common

characteristics, i.e., a microscopic deformation with reversible elasticity before an inflection point (less than 10% compression), a greater change in the sample length containing irreversible deformation of the materials after an inflection point (10–40% compression), and a rapid increase in the compressive stress accompanied by the development of numerous macroscopic cracks within the sample. Further compression cause the entire material to macroscopically collapse in some cases. Through the compression testing, the entire process can be traced from reversible microscopic deformation at the initial stage to irreversible macroscopic fracture at the final stage. It includes useful aspects beyond the information obtained from the tensile test.

For the compression curves of the epoxy monoliths in Fig. 8a, b, the strength value at the inflection point increases to 7.5 ± 0.3 MPa when 30 mol% TPGD was added, then it decreased to 3.9 ± 0.8 MPa with the further addition of TPGD. The strain values at the inflection point were 3.0–3.8% independent of the TPGD contents, except for the monolith that contained 50 mol% TPGD, for which the strain was 10.1%. At compressive strains less than 40%, the slopes of the curves were small for all samples. Under further compressed conditions, the stress rapidly increased. The epoxy monolith samples with a 5.5–6.5 mm height before compression were flattened to a 1.0–1.5 mm height just after compression, as shown in Fig. 8d. Simultaneously, the diameter increased from 4.0–4.1 mm as the initial size to 5.8–6.6 mm as the final size. The epoxy monolith was partially destroyed but not completely shattered. The epoxy monolith that contained 50 mol% TPGD exhibited compression characteristics similar to a typical rubbery material. The stress–strain curve increased over 40% compression, different from any other samples. As shown in the stress–strain curves for the bulk thermosets in Fig. 8c, the stress and strain values were 89.1–99.3 MPa and 9.5–12.2%, respectively, at the inflection points. The values were much higher than those for the epoxy monoliths. After the inflection point, some microscopic collapse of the materials occurred. The bulk thermoset samples prepared at $\gamma = 1.4$ were macroscopically crushed at ~70% compression, and the thermoset prepared at $\gamma = 1.0$ was more brittle and rapidly crashed at less than 50% compression. The compressive strain at break slightly increased when a small amount of TPGD was added, which was different from the monolith results obtained. The strength at break was 178–324 MPa for the bulk thermosets, which was approximately half the strength of the glassy epoxy monoliths (459–572 MPa). These results support that the monolith materials exhibit high performance derived from their unique co-continuous porous structure for energy dissipation during compression deformation.

Next, we investigated the cyclic compression behavior of the monoliths at different applied force conditions. As

Fig. 8 Stress–strain curves for the compression test of (a) monolith cylinders ($\gamma = 1.4$), (b) expanded curves for the initial region of (a), and (c) bulk thermosets ($\gamma = 1.4$ and 1.0). **d** Photographs of the test pieces of monoliths ($\gamma = 1.4$, TPGD = 0 and 10 mol%) and bulk thermosets ($\gamma = 1.4$ and 1.0, TPGD = 0 mol%) before and after (more than 1 week) the compression test

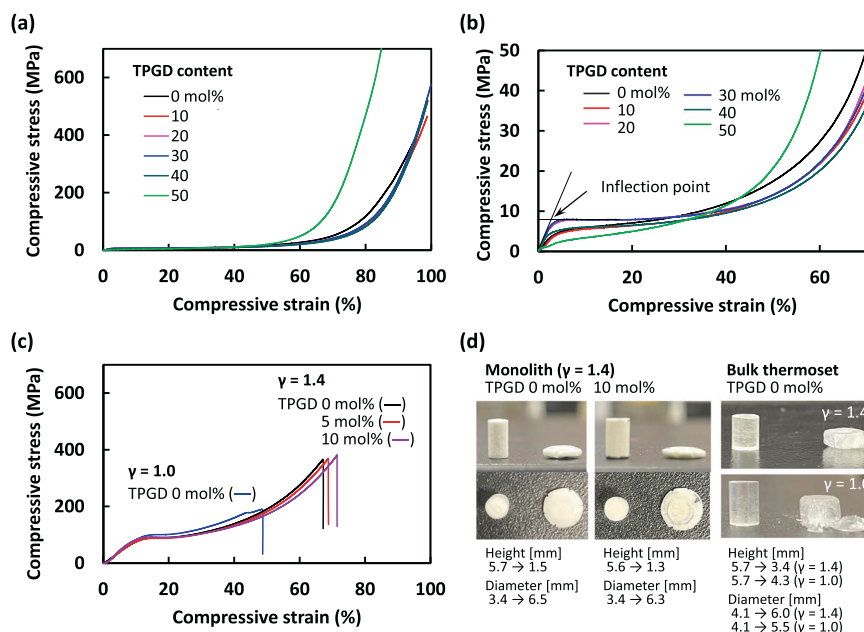


Table 3 Mechanical properties for the compression test of epoxy monoliths and bulk thermosets with various amount of TPGD^a

Material	TPGD content (mol%)	Young's modulus (MPa)	At the inflection point		At break		Slope (GPa)
			Strength (MPa)	Strain (%)	Strength (MPa)	Strain (%)	
Monolith ($\gamma = 1.4$)	0	153 ± 25	5.5 ± 0.3	3.8 ± 0.4	472 ± 11	98.7 ± 0.8	3.1 ± 0.2
	10	160 ± 15	5.0 ± 0.2	3.3 ± 0.5	459 ± 11	98.3 ± 0.8	2.9 ± 0.1
	20	229 ± 24	6.9 ± 0.7	3.0 ± 0.2	506 ± 24	98.4 ± 1.0	3.6 ± 0.2
	30	236 ± 25	7.5 ± 0.3	3.2 ± 0.5	572 ± 7	99.2 ± 1.2	4.2 ± 0.1
	40	168 ± 17	5.5 ± 0.2	3.1 ± 0.6	522 ± 3	96.8 ± 3.4	4.2 ± 0.1
	50	60 ± 38	3.9 ± 0.8	10.1 ± 7.8	820 ± 13 ^b	92.1 ± 4.1 ^b	5.9 ± 0.4 ^b
Bulk thermoset ($\gamma = 1.4$)	0	832 ± 144	90.1 ± 2.7	11.6 ± 1.6	231 ± 91	56.0 ± 8.9	^c
	5	826 ± 19	89.1 ± 2.3	11.4 ± 0.7	324 ± 31	66.5 ± 2.6	^c
	10	971 ± 90	91.6 ± 3.4	9.5 ± 1.2	289 ± 79	65.0 ± 4.4	^c
Bulk thermoset ($\gamma = 1.0$)	0	846 ± 15	99.3 ± 0.0	12.2 ± 0.4	178 ± 12	48.7 ± 0.0	^c

^aEpoxy monoliths and bulk thermosets were prepared using BADGE, TPGD, and BACM in the presence and absence of PEG, respectively, at 120 °C

^bNo break under the condition at the maximum applied force (5 kN) in this study

^cNot determined

shown in Fig. 9a, the epoxy monolith in principle exhibited elastic properties at the initial stage with an applied force less than 5 MPa. The curves gradually shifted in the more compressed direction, indicating that these cycles involve some degree of irreversible and plastic deformation. It was also clarified that the reversibility of deformation increased when a small amount of TPGD was added (Fig. 9b). When the range of applied force was extended to 0–10 MPa, the stress–strain curve passed the inflection point at ~5% strain and ca. 8 MPa stress and reached ca. 30% elongation (Fig. 9c). After the applied force was released, only several

percent of the strain was recovered for each cycle. It has also been revealed that these materials exhibited only weak creep properties (see Fig. S7 in the Supplementary Materials). The cyclic compression and relaxation behaviors under the conditions using holding times of 600 and 7200 s showed no significant difference in the stress–strain curves (Fig. S8a). At the final stage of compression, the recovery ratio increased, and the stress–strain curve followed the same trajectory (Fig. 9d). In contrast to the plastic deformation of the epoxy monoliths in the earlier stage before the inflection point, reversible compression behavior by the

Fig. 9 Cyclic stress–strain curves for the compression test of the epoxy monoliths at room temperature. Cycle number = 10, holding time 600 s. **a** TPGD 0 mol%, applied pressure range 0–5 MPa, **b** TPGD 10 mol%, applied pressure range 0–5 MPa, **c** TPGD 0 mol%, applied pressure range 0–10 MPa, and **d** TPGD 0 mol%, applied pressure range 0–30 MPa. The reaction conditions for the preparation of the epoxy monoliths were $\gamma = 1.4$, TPGD content 0 or 10 mol% at 120 °C for 1.5 h

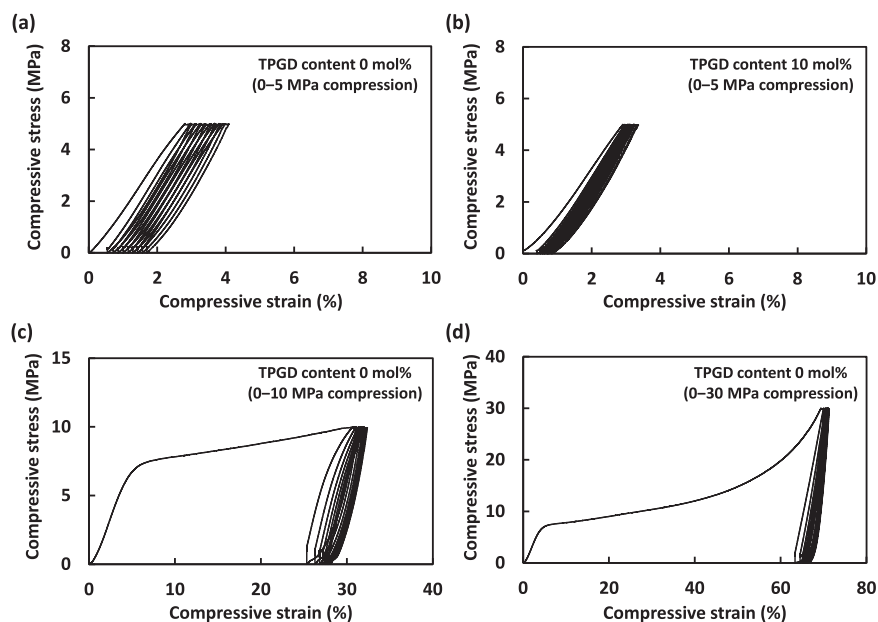
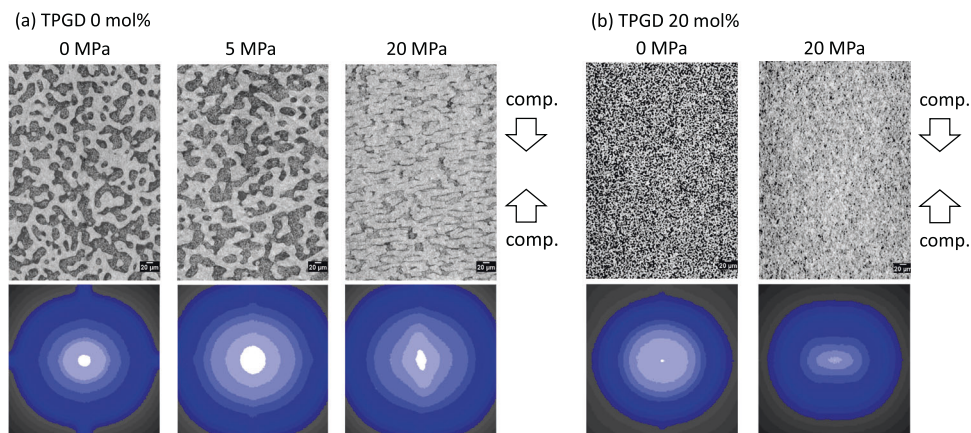


Fig. 10 Cross-sectional X-ray CT images (upper) and the results processed by fast Fourier transformation (FFT) (bottom) of the CT images for the inner structures of the epoxy monoliths prepared in the (a) absence and (b) presence of TPGD (20 ml%) before and after cyclic compression tests (10 cycles). Compression was performed with a direction of arrows



applied force and the subsequent release was observed for the bulk thermoset as a typical elastic material (Fig. S8b).

X-ray CT imaging

Furthermore, we directly evaluated the compressive deformation of the monoliths using X-ray CT imaging. The cross-sectional X-ray CT images for the inner structure of the epoxy monoliths prepared in the absence and presence of TPGD are shown in Fig. 10 (see also the movies as Videos S1–S5 in the Supplementary Materials). These images clearly indicate that a coarse monolith structure formed in the absence of TPGD in contrast to the fine porous structure produced in the presence of TPGD (20 mol%). The presence of many epoxy particles in the pores of the monolith was also confirmed in the CT images of Fig. 10a.

The sizes of the epoxy skeletons and pores depended on the TPGD content and the curing temperature. This result is

identical to the results described for the fabrication of epoxy monolith sheets [21]. The cross-sectional SEM images for the cylindrical monoliths prepared at different curing temperatures and TPGD contents under the γ condition of 1.4 are shown in Fig. S9 as supplementary materials. As the curing temperature increased, a monolith with a fine porous structure was produced. In addition, it was revealed that the formation of aggregates of epoxy globules as secondary phase separation products was suppressed by the addition of TPGD and the increase in curing temperature. Actually, no formation of particles was observed for the monolith manufactured in the presence of 20 mol% TPGD at 120 °C or without TPGD at 140 °C. Unfortunately, the pore sizes shown in Fig. 10b are too small for further investigation by X-ray CT imaging to clarify the compressive deformation behavior of the monoliths. It was also confirmed that curing at 100 °C could fabricate monoliths with a larger pore size, but many aggregates of epoxy globules were inevitably

formed as side products, even when TPGD (20 mol%) was added (Fig. S9).

When repeated pressure was applied at 5 MPa (the cycle number was 10), the macroscopic deformation was less than 2%, as shown in Fig. 9a. As a result, the original porous structure almost remained, even after compressive deformation (Fig. 10a). In contrast, the deformation at 20 MPa resulted in the irreversible deformation of the monolith structures. The largely flattened pores and the anisotropic deformation of the epoxy monolith skeletons were observed. It was difficult to discuss the deformation behavior for the fine monoliths produced in the presence of TPGD (Fig. 10b). To examine the anisotropic deformation of the monoliths by compression, we attempted to mathematically convert the CT images in a real space to the image in a reciprocal space by the fast Fourier transformation (FFT) technique [27]. As shown in Fig. 10, the images obtained after FFT processing reflect the anisotropic structure of the compressed monolith skeletons, including a stack of layered monoliths; i.e., concentric circles are observable in the FFT image for the monolith before compression, while the rings slightly collapse after repeated compression at 5 MPa, and the anisotropy increases after pressing at 20 MPa. The FFT image for the samples including 20 mol% TPGD provides any anisotropic structural information after compressive deformation, although the CT and FFT images are blurry. More detailed analysis of the FFT images is being continued, and the results will be reported in the future.

Conclusions

In this study, we prepared epoxy monoliths using BADGE and TPGD as epoxy resins combined with BACM as the crosslinker and PEG as the porogen. The sheet and cylindrical samples of the epoxy monoliths were subjected to mechanical tensile and compression tests, respectively, to clarify the effects of TPGD additions on the mechanical properties of the epoxy monolith. The tensile test of the monolith sheets revealed that the mechanical properties drastically changed when more than 20 mol% TPGD was added because the formation of aggregates of epoxy globules by the secondary phase separation mechanism was suppressed; in addition, several predictable effects occurred to soften the monolith and reduce the pore sizes. The compression test using cylindrical test pieces provided valuable information on the entire process from reversible microscopic deformation of the monolith skeletons at the initial stage of compression to irreversible macroscopic material fracture at the final stage. In addition, the X-ray CT imaging method provided valuable information on the structural changes in the inner structure of the epoxy monolith under applied compressive force conditions. The experimental data about the structural change in the epoxy

monolith tracked by X-ray CT imaging during compression deformation will be useful for determining the fracture mechanism of the epoxy monolith as well as composite materials, such as co-continuous polymer networks (CNPs), which are fabricated by filling the elastic network polymers into the pores of the epoxy monoliths [20, 21]. We are continuing to prepare epoxy monoliths and CNPs without secondary particle aggregation to clarify the detailed mechanism that underlies their fracture and toughening.

Compliance with ethical standards

Conflict of interest The authors declare no competing interests.

References

1. Petrie EM. Handbook of adhesives and sealants. 2nd ed. New York: McGraw-Hill; 2007.
2. Sprenger S. Epoxy resins modified with elastomers and surface-modified silica nanoparticles. *Polymer*. 2013;54:4790–7.
3. Jin F-L, Li X, Park S-J. Synthesis and application of epoxy resins: a review. *J Ind Eng Chem*. 2015;29:1–11.
4. Mashouf Roudsari G, Mohanty AK, Misra M. Green approaches to engineer tough biobased epoxies: a review. *ACS Sustain Chem Eng*. 2017;5:9528–41.
5. Kumar S, Krishnan S, Samal SK, Mohanty S, Nayak SK. Toughening of petroleum based (DGEBA) epoxy resins with various renewable resources based flexible chains for high performance applications: a review. *Ind Eng Chem Res*. 2018;57:2711–26.
6. Ahmadi Z. Nanostructured epoxy adhesives: a review. *Prog Org Coat*. 2019;135:449–53.
7. Wei H, Xia J, Zhou W, Zhou L, Hussain G, Li Q, et al. Adhesion and cohesion of epoxy-based industrial composite coatings. *Comp B*. 2020;193:108035.
8. Shundo A, Yamamoto S, Tanaka K. Network formation and physical properties of epoxy resins for future practical applications. *JACS Au*. 2022;2:1522.
9. Kinloch AJ. Mechanics and mechanisms of fracture of thermosetting epoxy polymers. *Adv Polym Sci*. 1985;72:45–67.
10. Chikhi N, Fellahi S, Bakar M. Modification of epoxy resin using reactive liquid (ATBN) rubber. *Eur Polym J*. 2001;38:251–64.
11. Kishi H, Matsuda S, Imade J, Shimoda Y, Nakagawa T, Furukawa Y. The effects of the toughening mechanism and the molecular weights between cross-links on the fatigue resistance of epoxy polymer blends. *Polymer*. 2021;223:123712.
12. Tanaka N, Kobayashi H, Nakanishi K, Minakuchi H, Ishizuka N. Monolithic LC columns. *Anal Chem*. 2001;73:420A–9A.
13. Aoki H, Tanaka N, Kubo T, Hosoya K. Polymer-based monolithic columns in capillary format tailored by using controlled in situ polymerization. *J Sep Sci*. 2009;32:341–58.
14. Nguyen AM, Irgum K. Epoxy-based monoliths. A novel hydrophilic separation material for liquid chromatography of biomolecules. *Chem Mater*. 2006;18:6308–15.
15. Tsujioka N, Ishizuka N, Tanaka N, Kubo T, Hosoya K. Well-controlled 3D skeletal epoxy-based monoliths obtained by polymerization induced phase separation. *J Polym Sci Part A Polym Chem*. 2008;46:3272–81.
16. Sakakibara K, Kagata H, Ishizuka N, Sato T, Tsujii Y. Fabrication of surface skinless membranes of epoxy resin-based mesoporous monoliths toward advanced separators for lithium-ion batteries. *J Mater Chem A*. 2017;5:6866–73.

17. Uehara F, Matsumoto A. Metal-resin bonding mediated by epoxy monolith layer. *Appl Adhes Sci.* 2016;4:18.
18. Sugimoto Y, Nishimura Y, Uehara F, Matsumoto A. Dissimilar materials bonding using epoxy monolith. *ACS Omega.* 2018;3:7532–41.
19. Sakata N, Takeda Y, Kotera S, Suzuki Y, Matsumoto A. Interfacial structure control and three-dimensional X-ray imaging of an epoxy monolith bonding system with surface modification. *Langmuir.* 2020;36:10923–32.
20. Tominaga R, Nishimura Y, Suzuki Y, Takeda Y, Kotera M, Matsumoto A. Co-continuous network polymers using epoxy monolith for the design of tough materials. *Sci Rep.* 2021;11:1431.
21. Tominaga R, Takeda Y, Kotera M, Suzuki Y, Matsumoto A. Non-destructive observation of internal structures of epoxy monolith and co-continuous network polymer using X-ray CT imaging for elucidation of their unique mechanical features and fracture mechanism. *Polymer.* 2022;263:125433.
22. Maire E, Withers PJ. Quantitative X-ray tomography. *Inter Mater Rev.* 2014;59:1–43.
23. Garcea SC, Wang Y, Withers PJ. X-ray computed tomography of polymer composites. *Comp Sci Technol.* 2018;156:305–19.
24. Mi Y, Zhou W, Li Q, Zhang D, Zhang R, Ma G, et al. Detailed exploration of structure formation of an epoxy-based monolith with three-dimensional bicontinuous structure. *RSC Adv.* 2015;5:55419.
25. Nakanishi K, Tanaka N. Sol-gel with phase separation. Hierarchically porous materials optimized for high-performance liquid chromatography separations. *Acc Chem Res.* 2007;40:863–73.
26. Svec F. Porous polymer monoliths: amazingly wide variety of techniques enabling their preparation. *J Chromatogr A.* 2010;1217:902–24.
27. Watanabe M, Takeda Y, Maruyama T, Ikeda J, Kawai M, Mitsumata T. Chain structure in a cross-linked polyurethane magnetic elastomer under a magnetic field. *Int J Mol Sci.* 2019;20:2879.

Publisher's note Springer Nature remains neutral with regard to jurisdictional claims in published maps and institutional affiliations.

Springer Nature or its licensor (e.g. a society or other partner) holds exclusive rights to this article under a publishing agreement with the author(s) or other rightsholder(s); author self-archiving of the accepted manuscript version of this article is solely governed by the terms of such publishing agreement and applicable law.